Supporting Information

Self-assembly of an α-Helical Peptide into a Crystalline Two-Dimensional Nanoporous Framework

Elizabeth L. Magnotti,[†⊥] Spencer A. Hughes,[†] Rebecca S. Dillard,[‡] Shengyuan Wang,[†] Lillian Hough,[†] Arshad Karumbamkandathil,[†] Tianquan Lian,[†] Joseph S. Wall,[§] Xiaobing Zuo,[¶] Elizabeth R. Wright,[‡] Vincent P. Conticello*

† Department of Chemistry, Emory University, Atlanta, Georgia 30322

‡ Department of Pediatrics, Emory University School of Medicine, Children's Healthcare of Atlanta, Atlanta, Georgia 30322

§Brookhaven National Laboratory, Upton, New York 11973

¶ X-Ray Science Division, Argonne National Laboratory, Argonne, Illinois 60439

*Corresponding author: vcontic@emory.edu

Contents

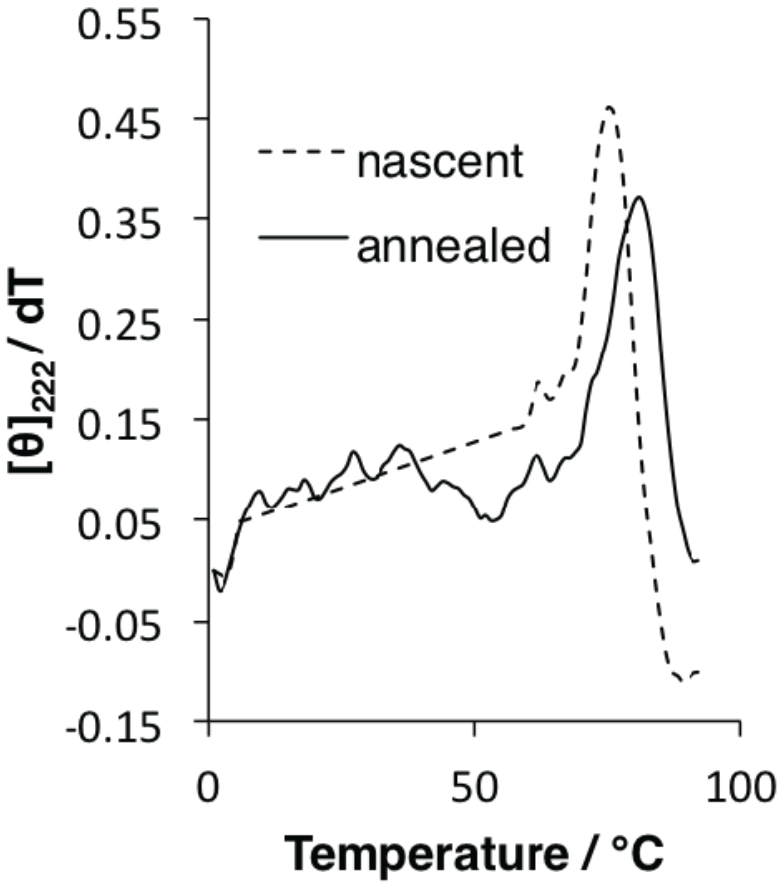

Figure S1. First derivative of the CD melting curves for nascent and thermally annealed solutions of **3FD-IL** (250 μM) in aqueous TAPS buffer (10 mM, pH8.5).

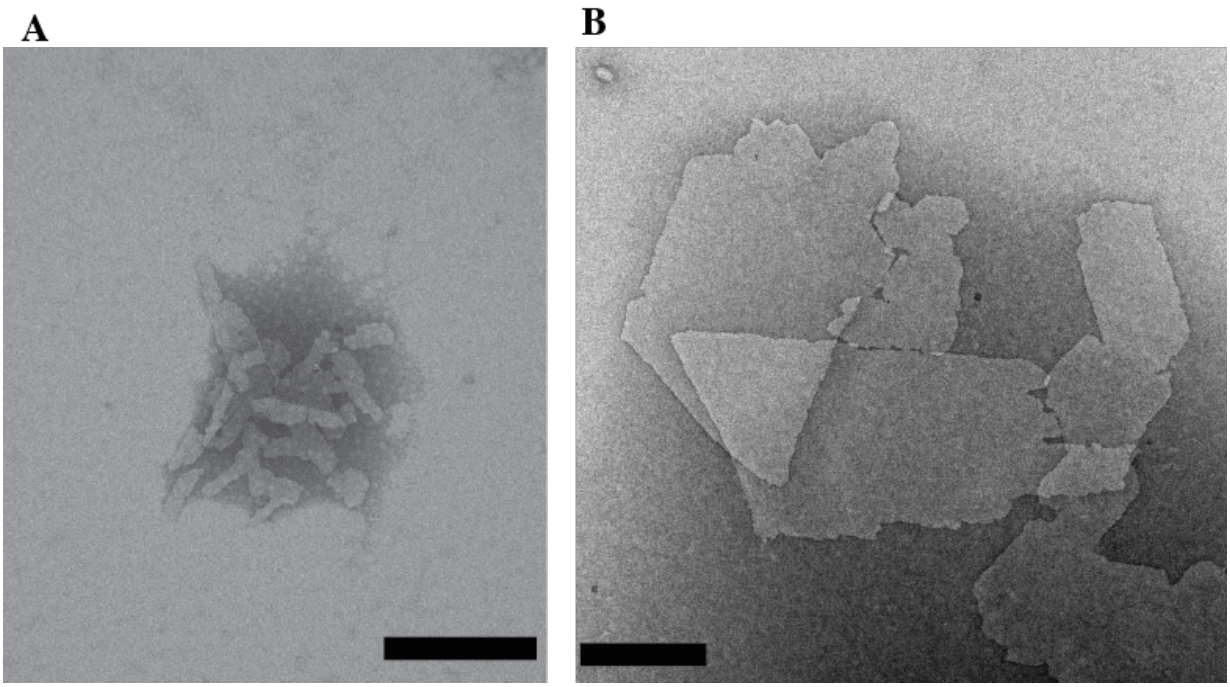

Figure S2. TEM images of nascent (**A**) and thermally annealed specimens (**B**) of **3FD-IL** nanosheet assemblies. Scale bar = 200 nm.

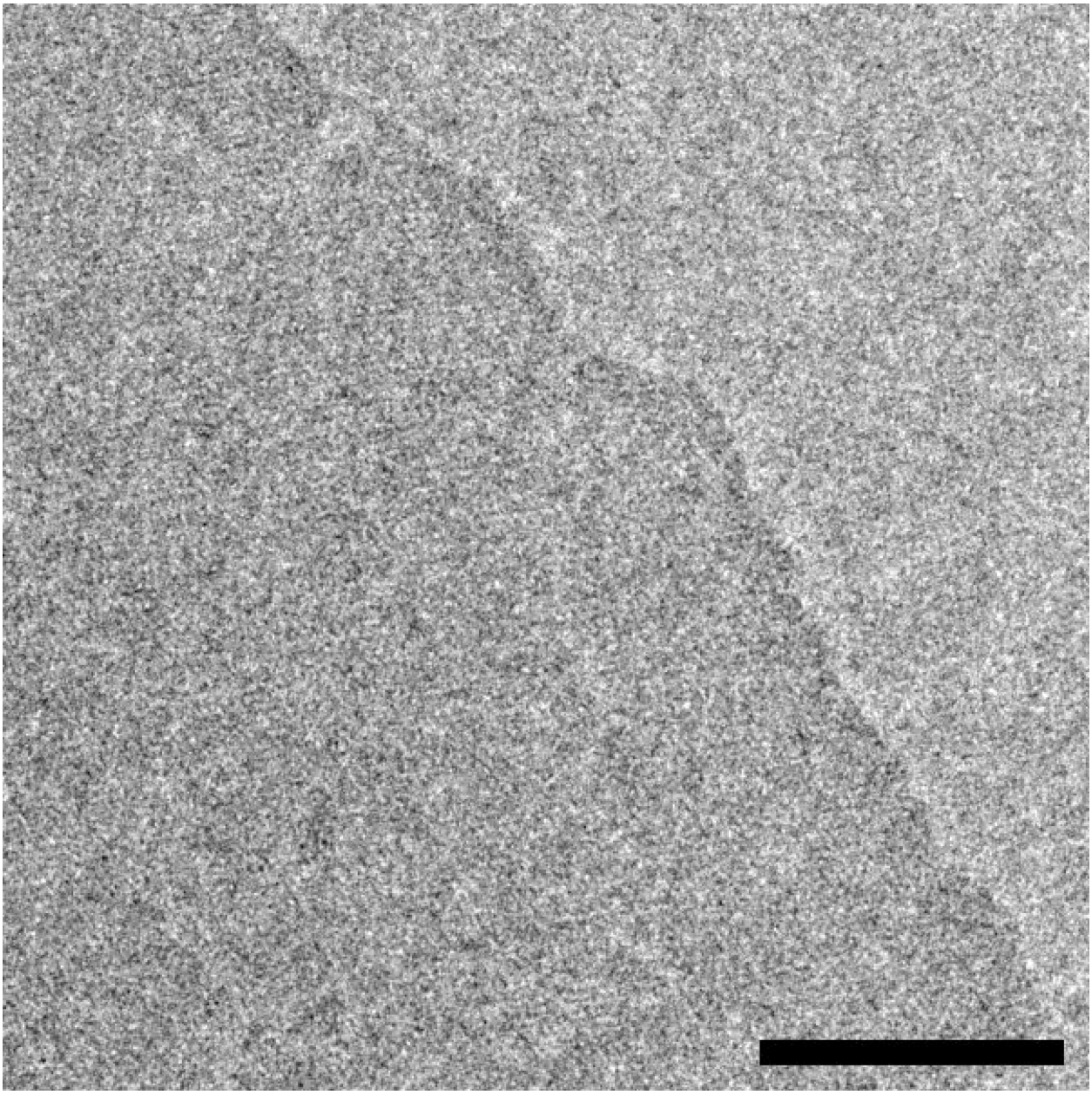

Figure S3. Magnification of a **3FD-IL** nanosheet from Figure 3b in which the periodic lattice of the sheet can be discerned on the left side of the boundary (scale bar = 50 nm). For comparison, the vitreous ice on the right side of the boundary lacks the features of the periodic lattice. Contrast was enhanced through use of a hole-free phase plate for phase imaging of the sample.

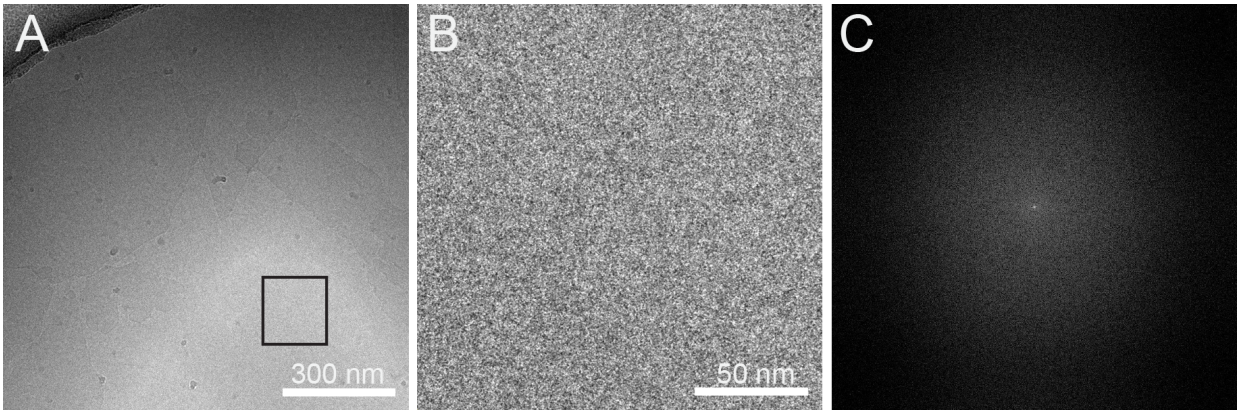

Figure S4. (**A**) Electron cryo-microscopy images of vitrified buffer samples. (**B**) Magnification of the boxed region in (**A**) indicating the absence of periodic lattice structure. (**C**) FFT revealing the lack of lattice structure.

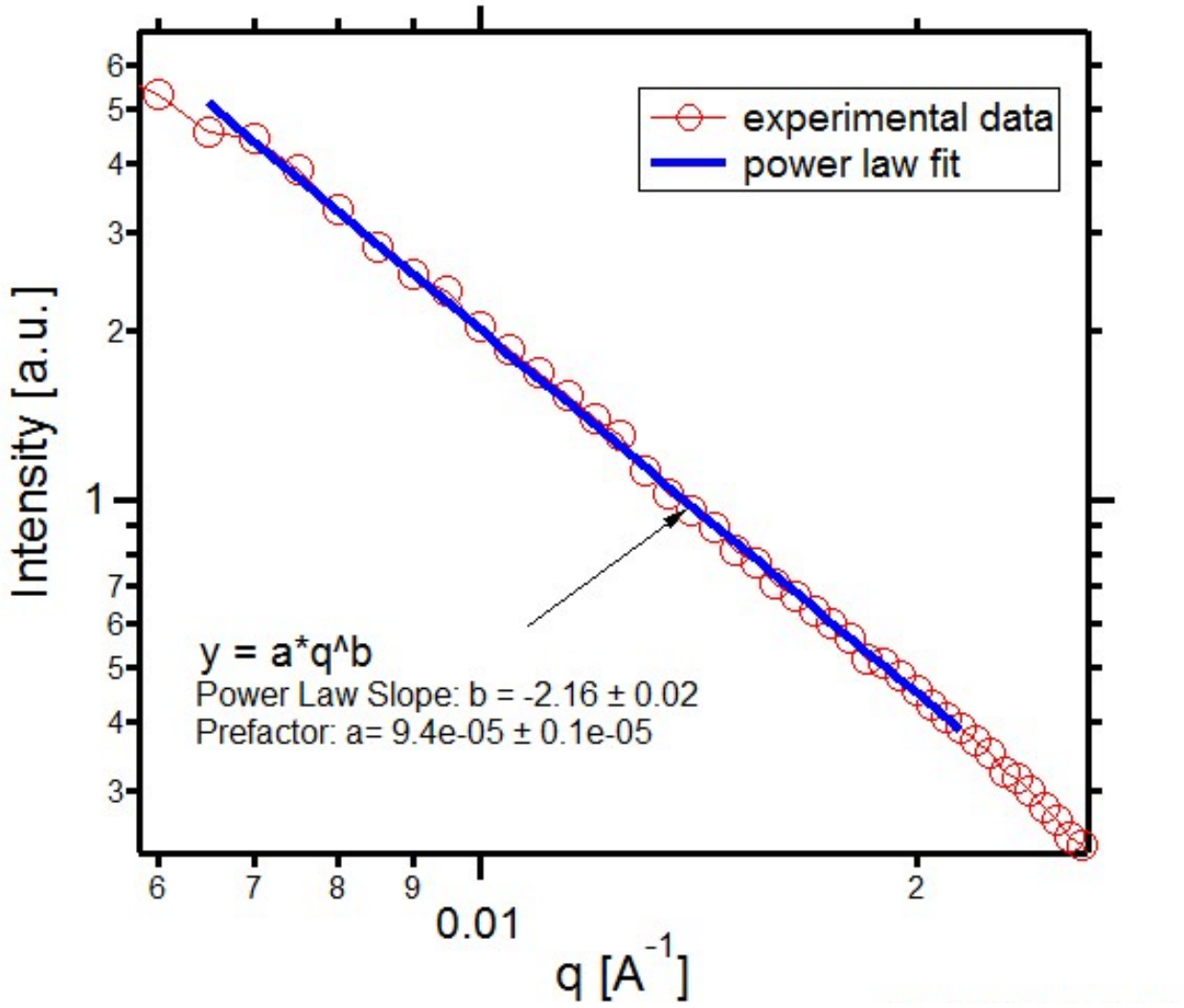

Figure S5. Power law fit of the experimental small angle X-ray scattering data for an aqueous solution **3FD-IL** (10 mg/mL) in aqueous TAPS buffer (10 mM, pH 8.5).

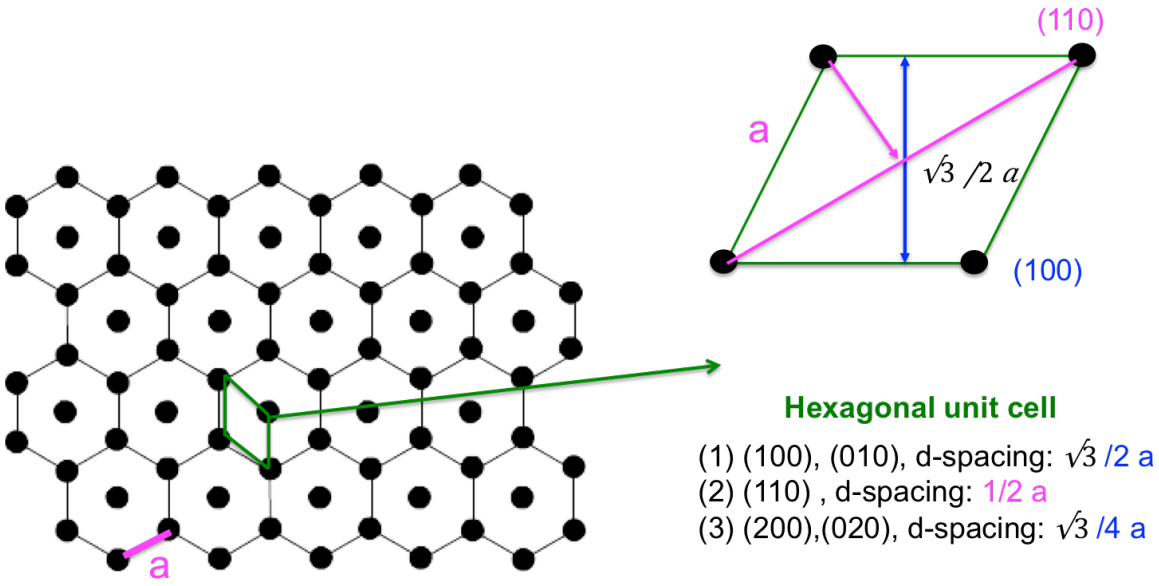

Figure S6. Structure model for the hexagonal close-packed lattice of **3FD-IL** helices (left). Helices are viewed in the direction of the helical axes (perpendicular to the surface of the sheet) and are represented as black dots. The unit cell is highlighted in green and shown in expanded form (upper right). The values for the lattice spacings are given in terms of the inter-helix distance of ca. 9.7 Å, which in a hexagonal close-packed structure corresponds to the unit cell parameter, **a** (lower right).

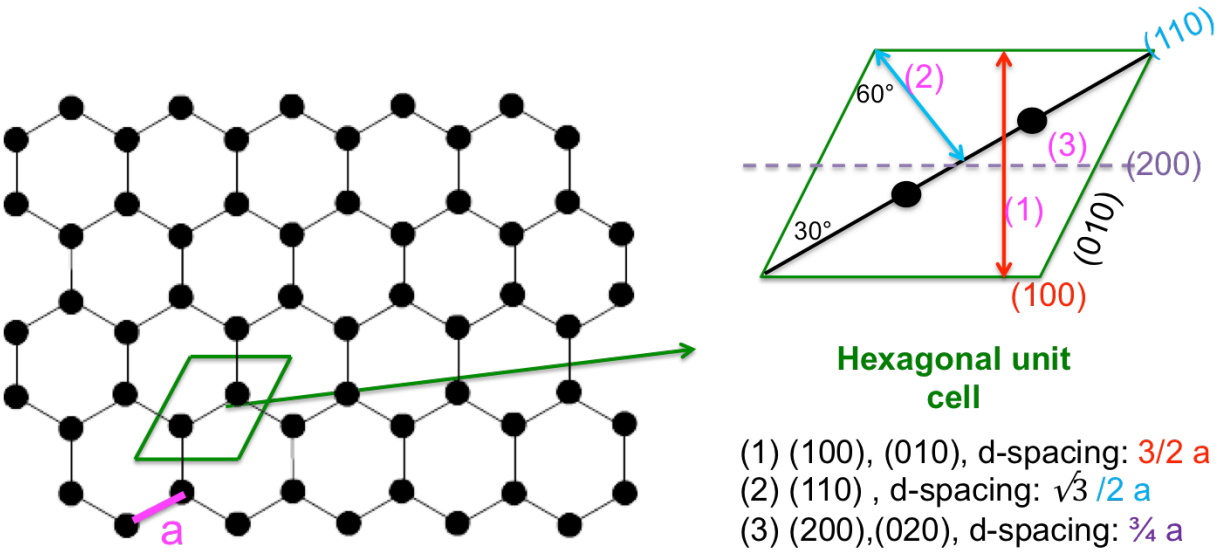

Figure S7. Structure model for the hexagonal honeycomb lattice of **3FD-IL** helices (left). Helices are viewed in the direction of the helical axes (perpendicular to the surface of the sheet) and are represented as black dots. The unit cell is highlighted in green and shown in expanded form (upper right). The values for the lattice spacings are given in terms of the inter-helix distance of ca. 9.7 Å, which in a hexagonal close-packed structure corresponds to the unit cell parameter, **a** (lower right).

A

3FD-IL-EKEK:

acetyl- E ALEKIA ALEKIA ALEKIA ALEKIA ALEKIA ALEKIA K-NH_2

3FD-IL-KEKE:

acetyl- E ALKEIA ALKEIA ALKEIA ALKEIA ALKEIA ALKEIA K-NH_2

3FD-IL-EEKK:

acetyl- E ALEEIA ALEEIA ALEEIA ALKKIA ALKKIA ALKKIA K-NH_2

B

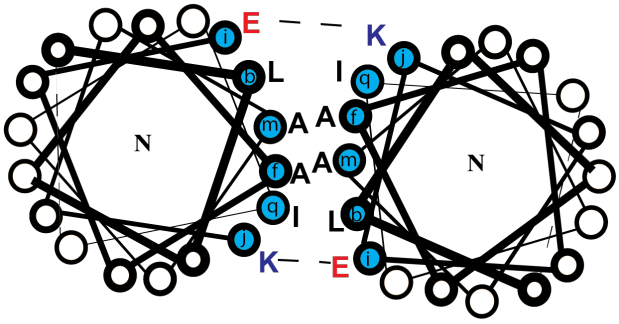

C

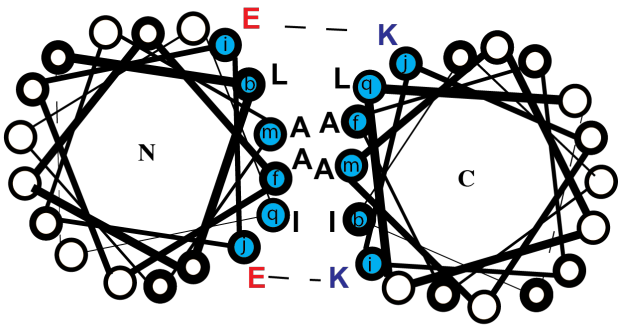

D

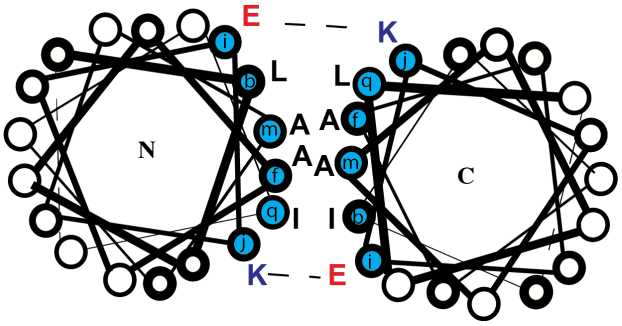

Figure S8. (**A**) Amino acid sequences of peptides **3FD-IL-EKEK**, **3FD-IL-KEKE**, and **3FD-IL-EEKK** with negatively charged glutamic acid residues (E) and positively charged lysine residues (K) highlighted in red and blue, respectively. (**B**) Helical wheel diagram depicting the complementary electrostatic interactions between charged residues at a helix-helix interface for **3FD-IL-EKEK** in a parallel orientation. (**C**) Helical wheel diagram depicting the complementary electrostatic interactions between charged residues at a helix-helix interface for **3FD-IL-EEKK** helices in an anti-parallel orientation. (**D**) Helical wheel diagram depicting the complementary electrostatic interactions between charged residues on a **3FD-IL-EKEK** helix (left) and a **3FD-IL-KEKE** helix (right) in an antiparallel orientation

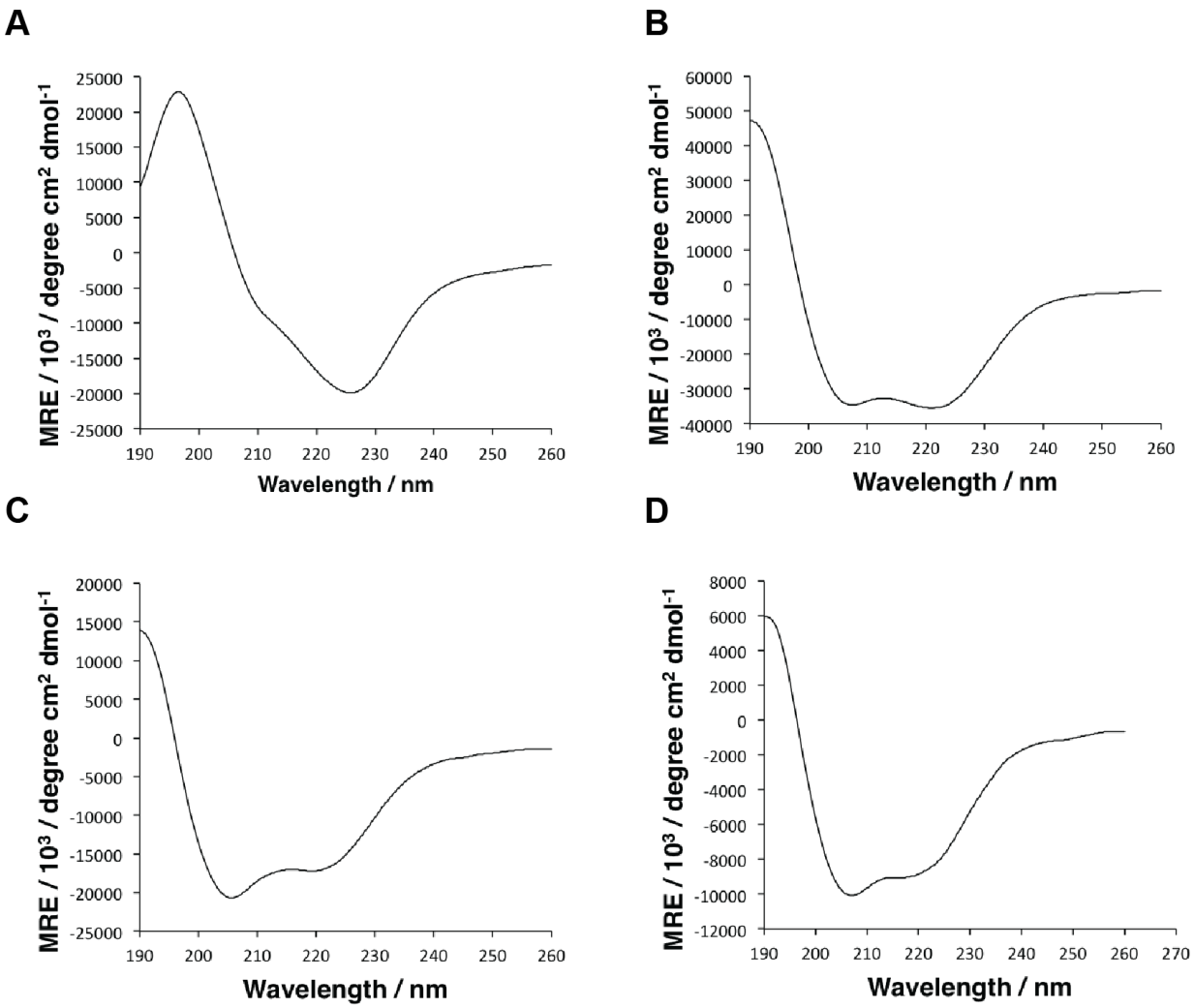

Figure S9. Circular dichroism spectra of thermally annealed solutions of (**A**) **3FD-IL-EEKK**, (**B**) **3FD-IL-EKEK**, (**C**) **3FD-IL-KEKE**, and (**D**) a 1:1 mixture of **3FD-IL-EKEK** and **3FD-IL-KEKE** at total peptide concentration of 250 μM in aqueous TAPS buffer (10 mM, pH 8.5).

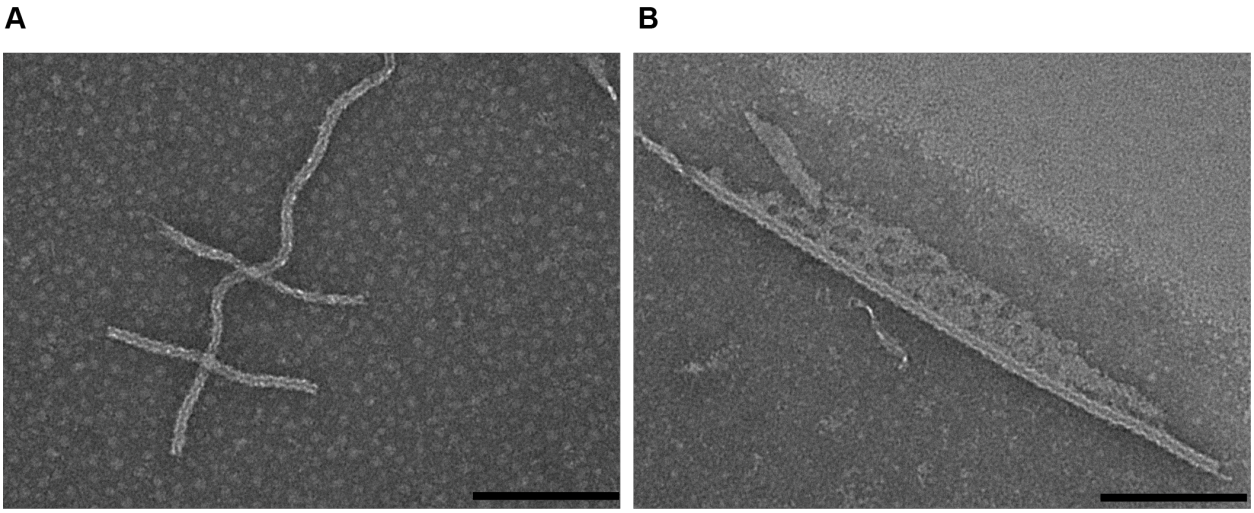

Figure S10. Transmission electron micrograph of representative fibrillar species formed from self-assembly of a thermally annealed solution of **3FD-IL-EKEK** (3 mg/mL) in aqueous TAPS buffer (10 mM, pH 8.5). Scale bar = 200 nm.

A

B

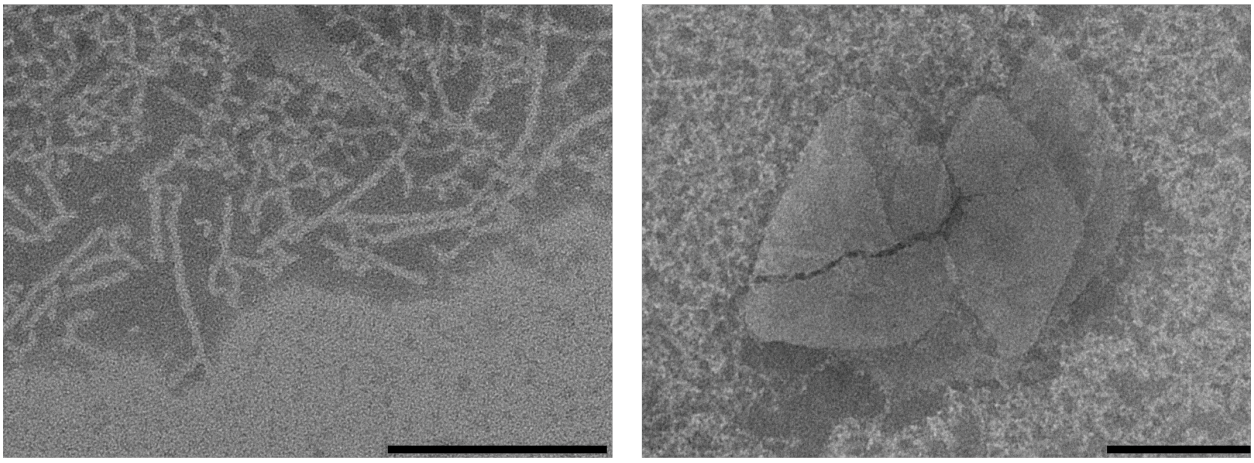

Figure S11. TEM images of a representative population of species that result from self-assembly of a thermally annealed solution of **3FD-IL-KEKE** (3 mg/mL) in aqueous TAPS buffer (10 mM, pH 8.5). Scale bar = 200 nm.

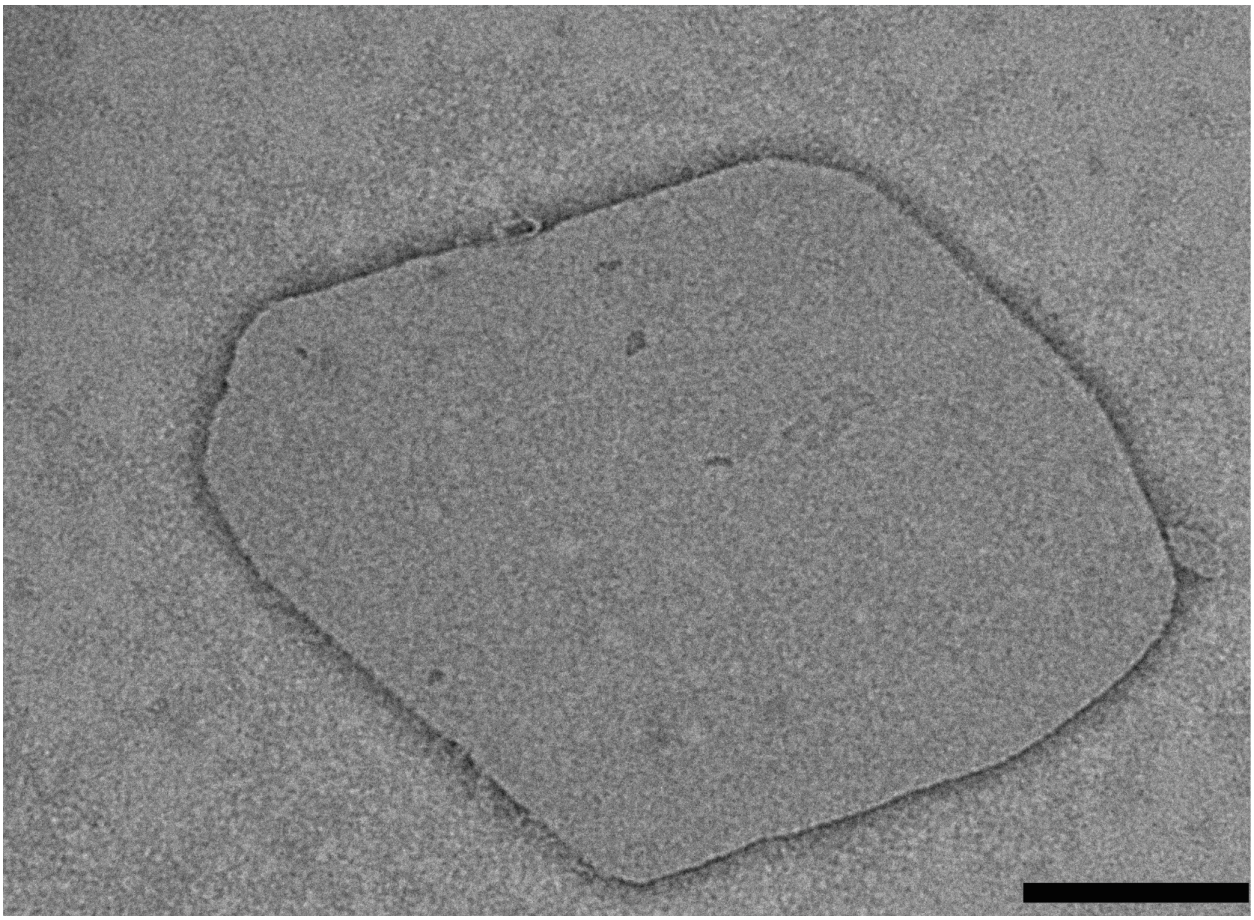

Figure S12. TEM image of a representative nanosheet that resulted from self-assembly of a thermally annealed solution of **3FD-IL-EEKK** (3 mg/mL) in aqueous TAPS buffer (10 mM, pH 8.5). Scale bar = 200 nm.

A

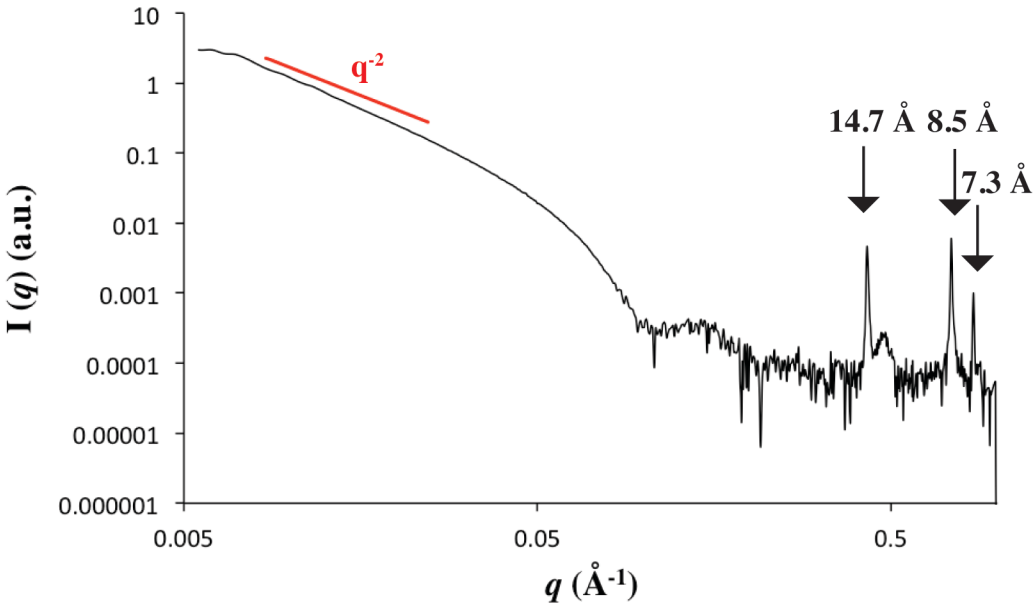

B

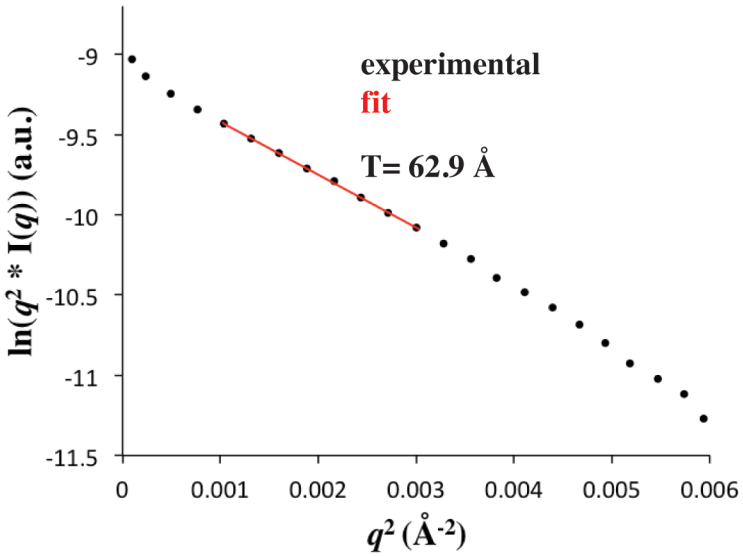

Figure S13. (A) Small-angle x-ray scattering curve for a thermally annealed solution of **3FD-IL-EEKK** nanosheets (10 mg/mL) in aqueous TAPS buffer (10 mM, pH 8.5). (B) Guinier fit of the scattering data for nanosheets of **3FD-IL-EEKK** using an equation for sheet-like forms, which yielded an experimental sheet thickness of 62.9 Å.

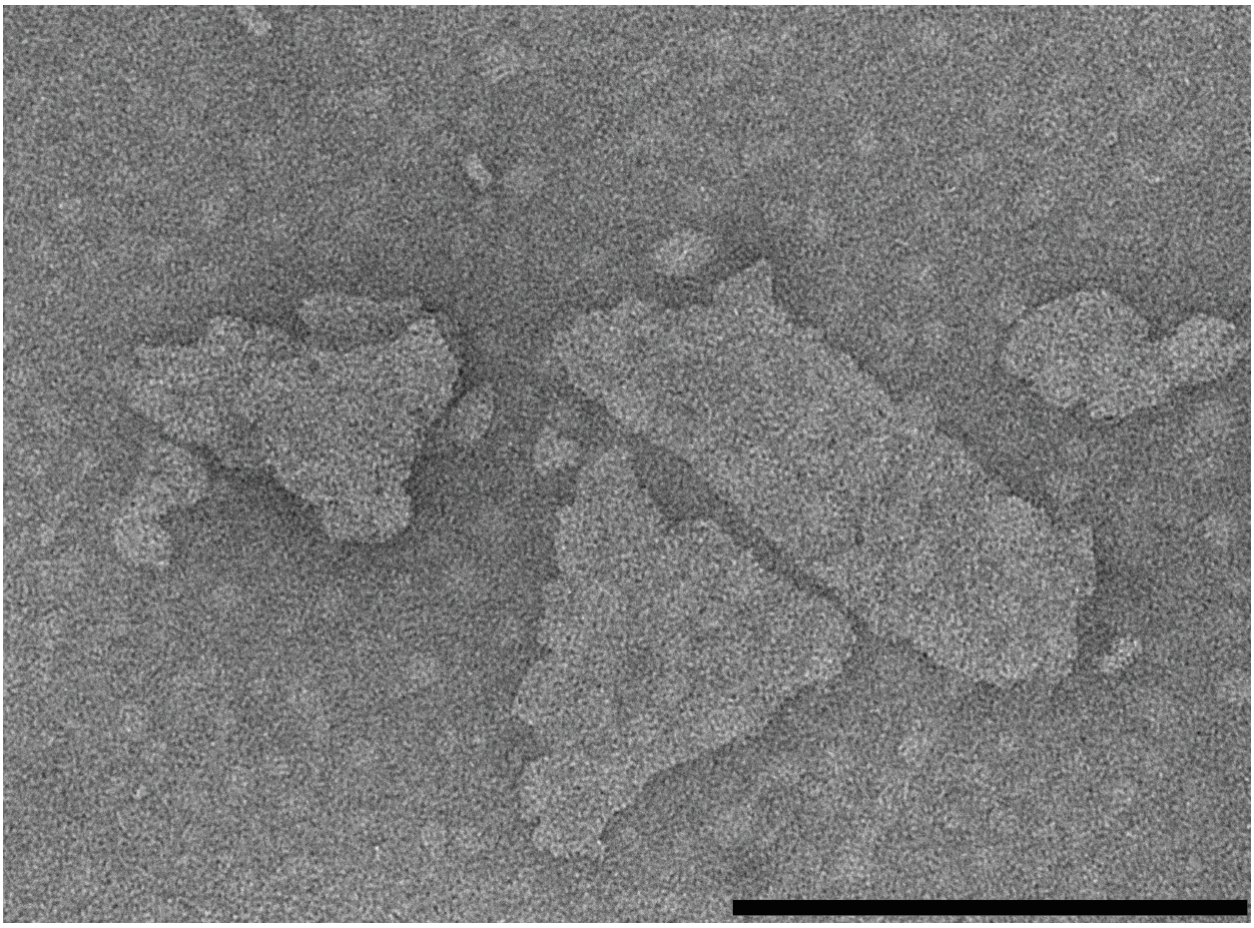

Figure S14. TEM image of representative nanosheets that result from self-assembly of a thermally annealed 1:1 mixture of **3FD-IL-EKEK** and **3FD-IL-KEKE** (total peptide concentration of 3 mg/mL) in aqueous TAPS buffer (10 mM, pH 8.5). Scale bar = 200 nm.

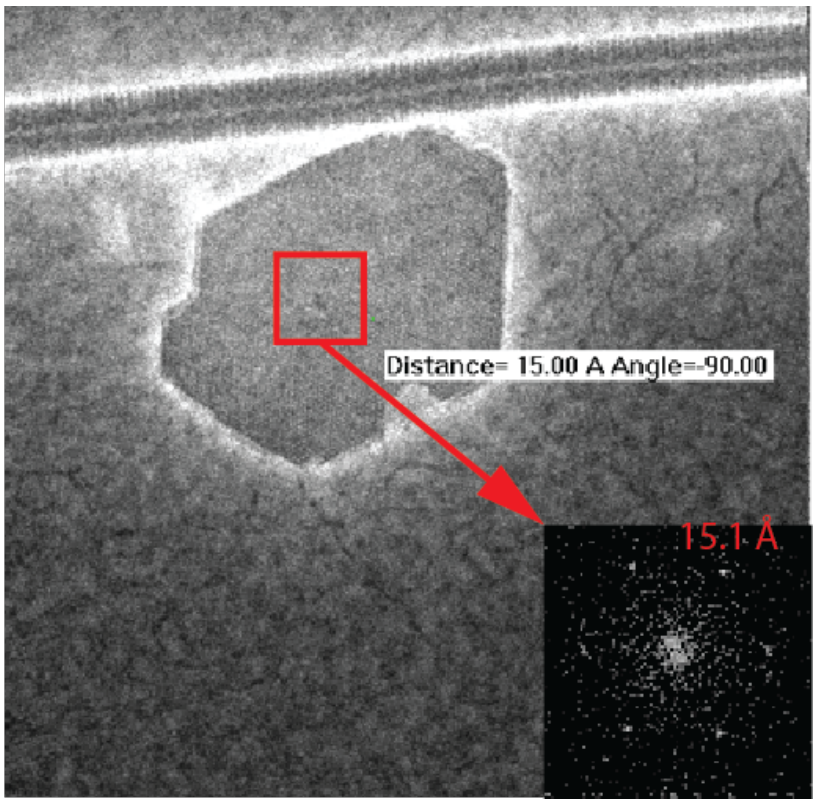

Figure S15. Negative-stain STEM image of a representative nanosheet of **3FD-IL**; the rodlike structure corresponds to tobacco mosaic virus. Inset: FFT of the STEM image that reveals the presence of a periodicity of 15.1 Å having hexagonal symmetry.

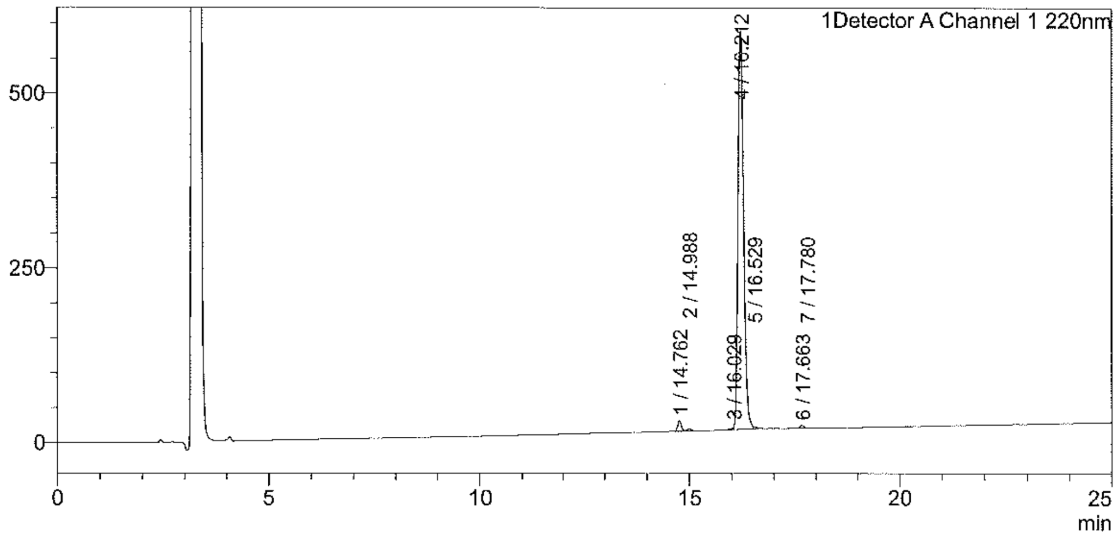

Figure S16. Analytical HPLC trace of peptide **3FD-IL**.

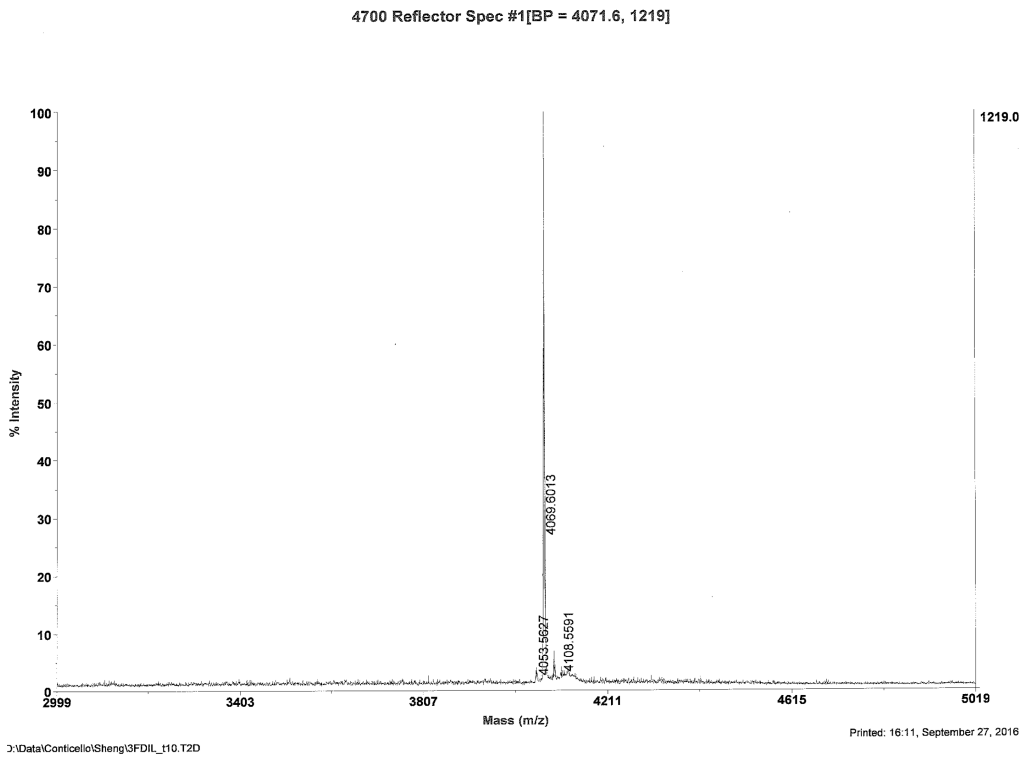

Figure S17. MALDI-TOF mass spectrum of peptide **3FD-IL**.

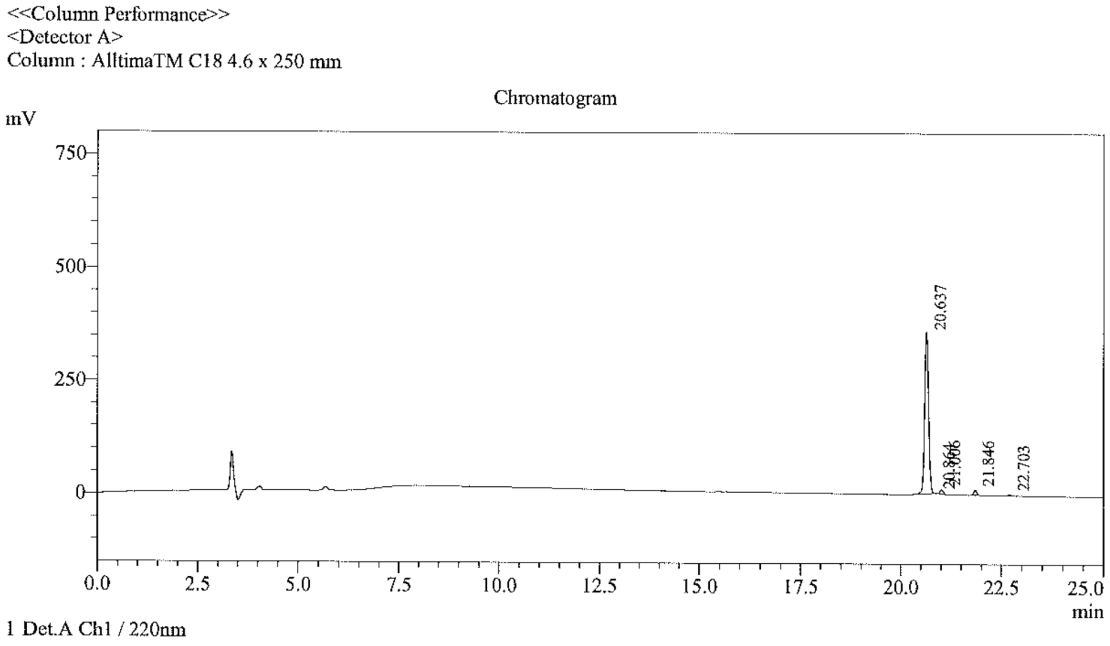

Figure S18. Analytical HPLC trace of peptide **3FD-IL-EKEK**.

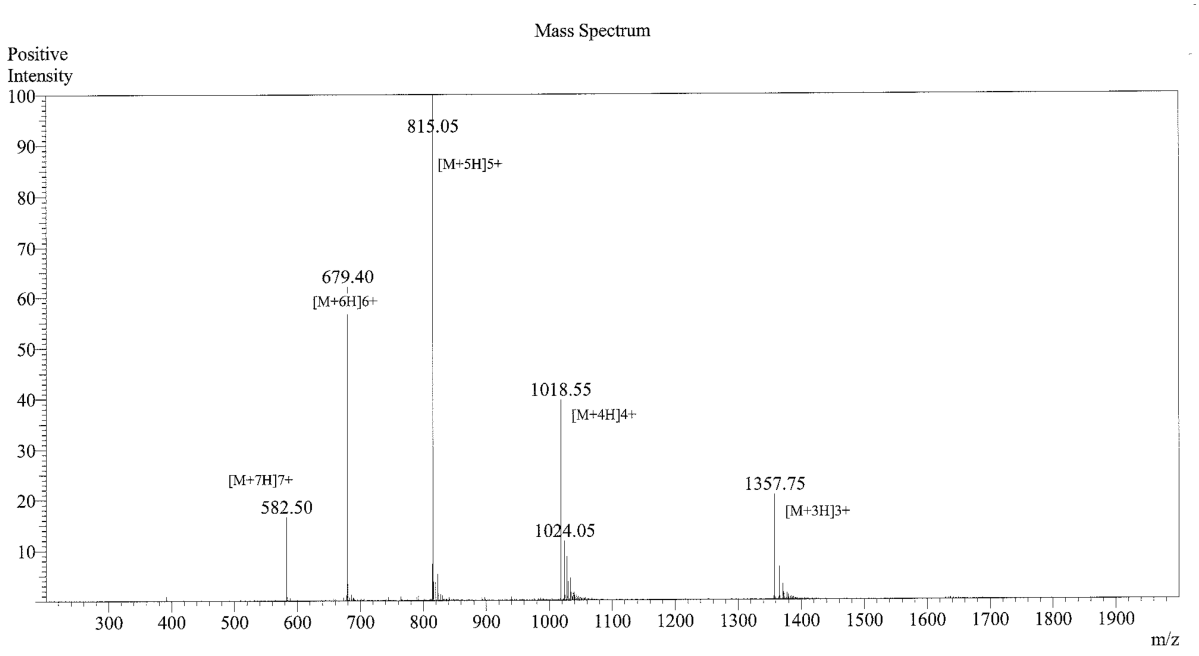

Figure S19. ESI-mass spectrum of peptide **3FD-IL-EKEK**.

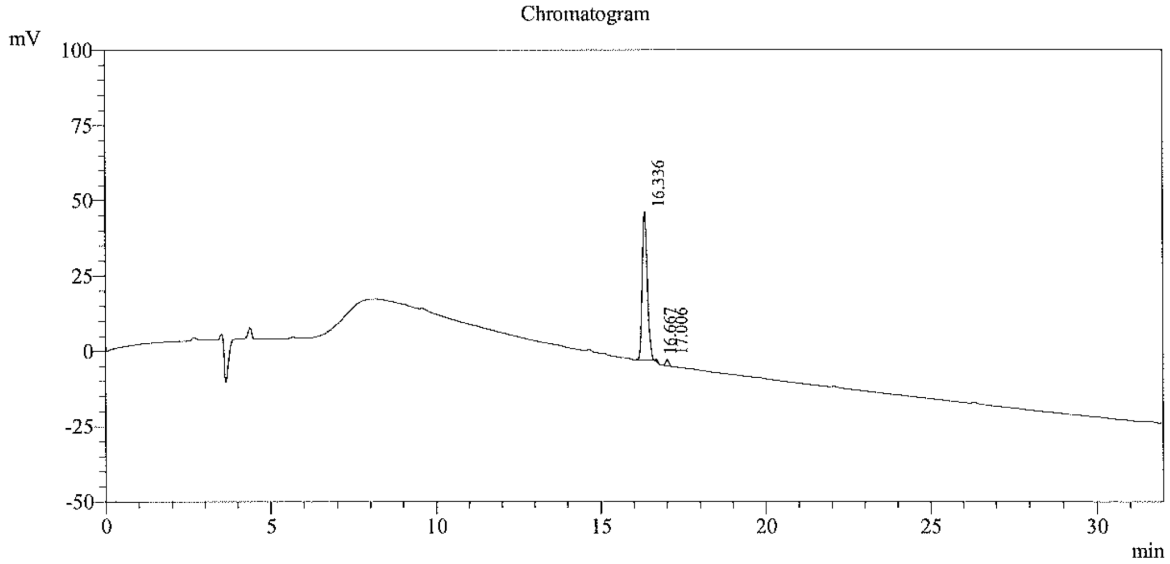

Figure S20. Analytical HPLC trace of **3FD-IL-KEKE**.

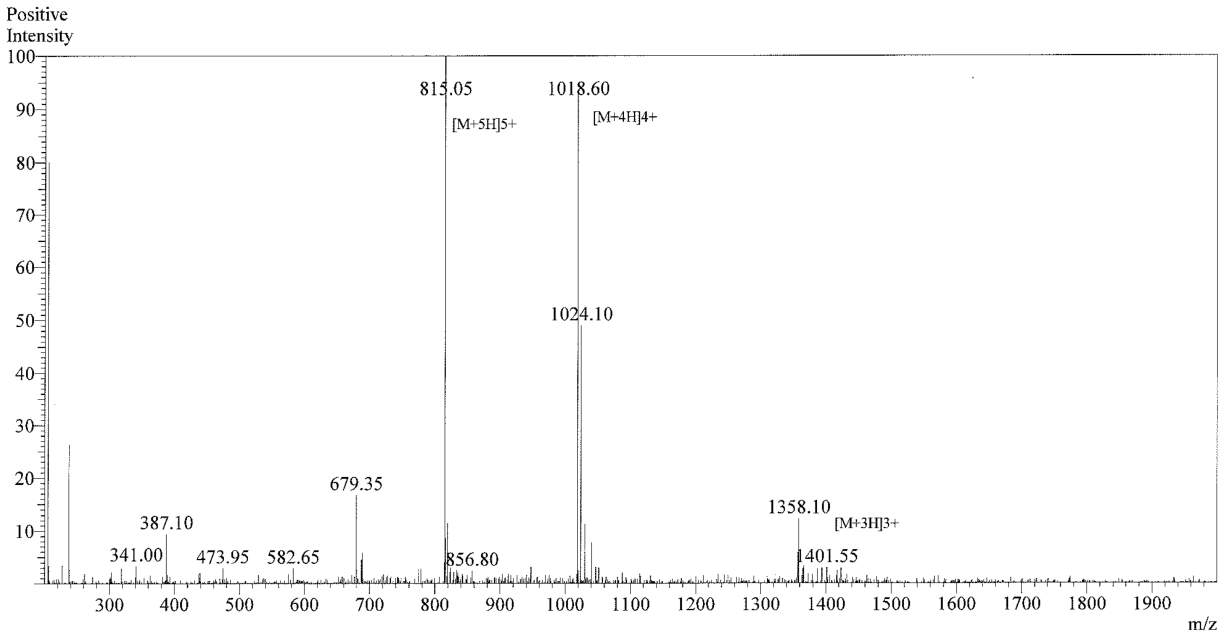

Figure S21. ESI-mass spectrum of peptide **3FD-IL-KEKE**.

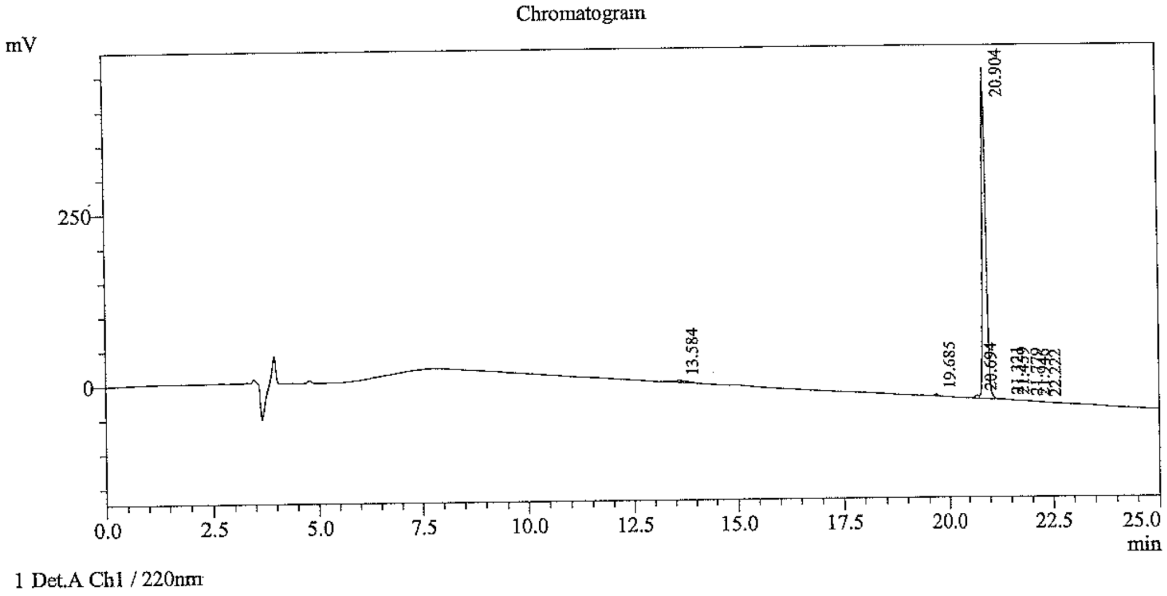

Figure S22. Analytical HPLC trace of **3FD-IL-EEKK**.

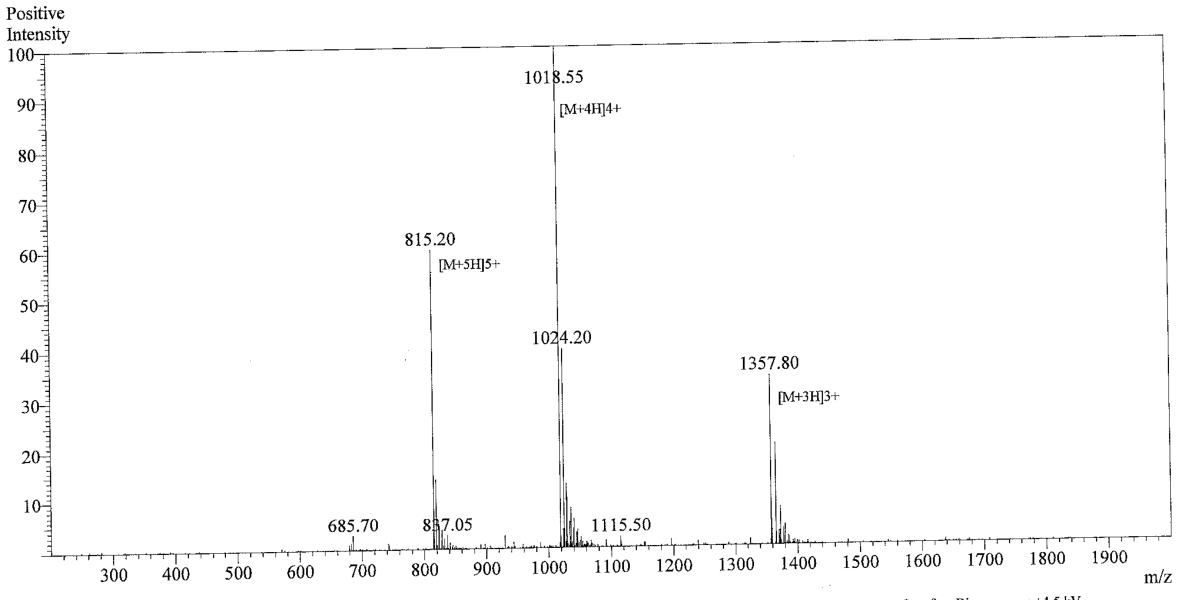

Figure S23. ESI-mass spectrum of peptide **3FD-IL-EEKK**.